

## Photometry and Spectroscopy of CI Camelopardalis from 1998–2005

E. A. Barsukova<sup>1</sup>, N. V. Borisov<sup>1</sup>, A. N. Burenkov<sup>1</sup>,  
V. P. Goranskii<sup>2</sup>, V. G. Klochkova<sup>1</sup>, and N. V. Metlova<sup>2</sup>

<sup>1</sup>*Special Astrophysical Observatory, Russian Academy of Sciences, Nizhniĭ Arkhyz,  
Karachaĭ-Cherkessian Republic, 369167 Russia*

<sup>2</sup>*Sternberg Astronomical Institute, Universitetskĭĭ pr. 13, Moscow, 119992 Russia*

Received August 18, 2005; in final form, November 14, 2005

**Abstract**—Our long-time monitoring of the B[e] star and transient X-ray source CI Cam during quiescence following the 1998 outburst demonstrates that the complex, stratified circumstellar envelope has tended to stabilize after this structure was perturbed by the passage of a shock wave from the outburst. The star's *UBVR* brightness shows slow, possibly cyclic, variations with an amplitude of about  $0.2^m$ . We determined the spectral type of the primary, B4III–V, based on the widths of the absorption wings of high-numbered Balmer lines. A Doppler shift of 460 km/s was detected for the HeII  $\lambda 4686 \text{ \AA}$  emission line. The shifts in this line yield an orbital period of 19.41 days, which is also manifested itself in the photometric data as a wave with a *V* amplitude of  $0.034^m$ . The orbit is elliptical, with an eccentricity of 0.62. It is most likely that the secondary is a white dwarf surrounded by an accretion disk. The primary's mass exceeds  $12 M_{\odot}$ . The system may be at a late stage of its evolution, after the stage of mass exchange.

PACS numbers : 97.30.Eh, 97.80.Jp

DOI: 10.1134/S1063772906080075

### 1. INTRODUCTION

CI Cam (XTE J0421+560) is a well-known B[e] star ( $V = 11.6^m$ ) and X-ray system. B[e] stars are an inhomogeneous class of stars with bright hydrogen and helium emission lines observed against a blue continuum; numerous emission lines of FeII and other metals, mainly in low ionization states and with low excitation potentials; forbidden emission lines of metals and light elements ([FeII], [NII], [OI]) in the optical; and strong infrared excesses due to emission from hot circumstellar dust [1]. These features are displayed by hot stars in various stages of their evolution, which may be attributed to in the same group due to the similar structures of their envelopes: pre-main-sequence Herbig Ae/B[e] stars, symbiotic stars, B[e] supergiants, compact planetary nebulae, and stars with warm dust. These features should probably be thought of as the B[e] phenomenon that are characteristic of various stellar classes.

In April, 1998, CI Cam experienced a strong outburst from gamma-ray to radio wavelengths, attracting attention to this star, and, more generally, to the B[e] phenomenon. The maximum X-ray brightness at 2–12 keV was 2 Crabs, and was achieved on April 1 at  $0^{\text{h}}57^{\text{m}}$  UT (JD 2450904.54). This outburst was unique among B[e] stars. The star's spectroscopic and photometric behavior during the outburst and

the first three years that followed are described by Barsukova et al. [2] and in [3–5]. At the outburst peak, the star's continuum brightness increased by at least an order of magnitude; the intensities of the hydrogen and FeII emission lines increased by factors of 5–10, of the HeI emission by a factor of 15–50, and of the HeII emission by a factor of 300, compared to the quiescent levels. At the same time, the flux in the [NII] forbidden line during the outburst did not differ from the flux in quiescence, although it increased by a factor of 1.5 somewhat later (after 50–250 days). Five behavior types were described for various spectral lines, which provide evidence for stratification in the dense circumstellar gas and dust envelope, which is supplied by stellar wind [2]. Photometry and measurements of the hydrogen-line intensities in quiescence following the outburst demonstrated slow cyclic brightness variations, with a cycle of 1100 days and an amplitude of 25–43%. It was suggested in [2] that these cyclic variations were related to the orbital motion of the system's cool component (G8II [6] or K0II [7]), and that the system was a symbB[e] symbiotic star. However, the presence of a cool component in the system was not confirmed by recent optical and infrared spectroscopic data, and the cyclic character of the variations requires confirmation over a time interval longer than three years.

Even after seven years of intensive study, informa-

tion about CI Cam remains contradictory. The distance to the star is unknown. Arguments for the distance being both small (1–2 kpc) [3, 8–11] and large (5–17 kpc) [4, 5, 12, 13] have been presented; an intermediate value,  $\approx 2.5$  kpc, is preferred in [14]. Many things depend on distance: the nature of the system's components, energy estimates, and the most likely origin of the 1998 outburst. According to recent studies [4, 5, 12], the optical component is a B0–B3 supergiant, while the compact component could be a black hole, neutron star, or a white dwarf. A supercritical accretion event onto a black hole or neutron star [4] and a thermonuclear explosion on the surface of a white dwarf (the outburst mechanism for classic novae [11, 12]) have both been considered as origins of the outburst. The contribution of the circumstellar envelope is very large in the optical and infrared, while the presence of the stellar components is almost negligible in the spectrum. According to [14], no photospheric lines have been found, even in high-resolution spectra ( $R \approx 60\,000$ ). The spectral energy distribution of the CI Cam based on far-ultraviolet HST spectroscopy coincides with that for a B3IV star after allowing for interstellar reddening,  $E(B - V) = 0.85^m \pm 0.05^m$  [5]. Broad photospheric absorption lines found in high order Balmer lines, which are most prominent for H $\delta$  and H $\epsilon$  [4]. The widths of hydrogen lines depend on the density of the material in the photosphere (the Stark effect). Lines formed in the atmospheres of supergiants are narrower than lines in the spectra of main-sequence stars. The widths of the hydrogen line wings in the spectrum of CI Cam contradict the conclusion of [4] that the system's B[e] component is a supergiant. However, Hynes et al. [4] did not undertake a detailed diagnostics of the hydrogen lines “because of the heavy contamination... in the wings of the lines (both in terms of other lines and also probably residual wind emission).”

The first VLA observations showed that the synchrotron radio source associated with the CI Cam outburst consisted of a central “core” and oppositely directed flows, which became S-shaped after some time [15] (the radio map was published in [16]). The star was accordingly included in lists of so-called “microquasars.” However, these VLA results were revised due to a claimed calibration error, and the star was removed from the list of microquasars [17]. The evolution of the outburst's radio remnant revealed by VLBA observations is described in [13]. It had a cloud-like structure resembling an edge-brightened shell, which expanded with deceleration. This structure is reminiscent of a shock wave moving in a dense interstellar medium. According to [13], it may still be possible to explain the radio nebula as the product of

a high-velocity jet if the motion of the jet material was quickly smothered by the dense surrounding medium.

The nature of the photometric variations with the 11.7-day period discovered by Miroshnichenko [7] in the observations of CI Cam acquired before the outburst [18] remained unclear. Our analysis of the same observations confirms the period, with amplitudes of  $0.16^m$ ,  $0.13^m$ , and  $0.10^m$  in the *BVR* bands. Barsukova et al. [2] confirmed the presence of this periodicity with a smaller amplitude,  $0.03^m$  in the *V* band, in their three-year observations after the 1998 outburst. Barsukova et al. [2] related the 11-day periodic brightness variations to the S-shaped radio jets [16] in a model with a rotating white dwarf with a bipolar magnetic field. The retraction of the report of radio jets [19] makes this model unnecessary. Furthermore, long-time monitoring [17] during 1999 (259 observations) did not confirm the presence of a 11.7-day period. These observations revealed instead irregular variations with an amplitude of  $0.2^m$ , a slow trend, and a “miniature” outburst.

In quiescence, CI Cam remains a weak, strongly variable X-ray source, whose X-ray spectrum contains soft and hard components separated at 2–3 keV and a bright Fe K $\alpha$  emission line. Its X-ray variability in quiescence is associated with rapid brightness fluctuations [19] and rapid changes of the HeI emission intensity [2, 4].

Our photometric and spectroscopic monitoring of CI Cam in quiescence from 1998–2001 [2] was continued until 2005; this paper presents the results of our seven-year observations. We organized special frequent photometric observations during 28 nights in November–December 2002 to check for the presence of the 11.7-day period, as well as spectroscopic observations in the blue with the 6 m telescope of the Special Astrophysical Observatory (SAO) and the UAGS spectrograph, for diagnostics of high-numbered Balmer-line profiles. We used our combined data to derive the orbital elements for the CI Cam system; preliminary results on the orbit appeared in [20].

## 2. PHOTOMETRIC OBSERVATIONS

Our photoelectric photometry was carried out by N.V. Metlova at the Sternberg Astronomical Institute (SAI)'s Crimean Station using the 60 cm Zeiss telescope with a single-channel *UBV* photometer designed by V.M. Lyutyi. As in [2], the comparison star was GSC 3723.54 ( $V = 10.401^m$ ,  $B - V = 0.759^m$ , and  $U - B = 0.336^m$ ), and the control star was GSC 3723.104 ( $V = 12.386^m$ ,  $B - V = 0.617^m$ , and  $U - B = 0.408^m$ ). The magnitudes of these stars were determined via comparison to the North Polar Sequence. We used these observations, which were

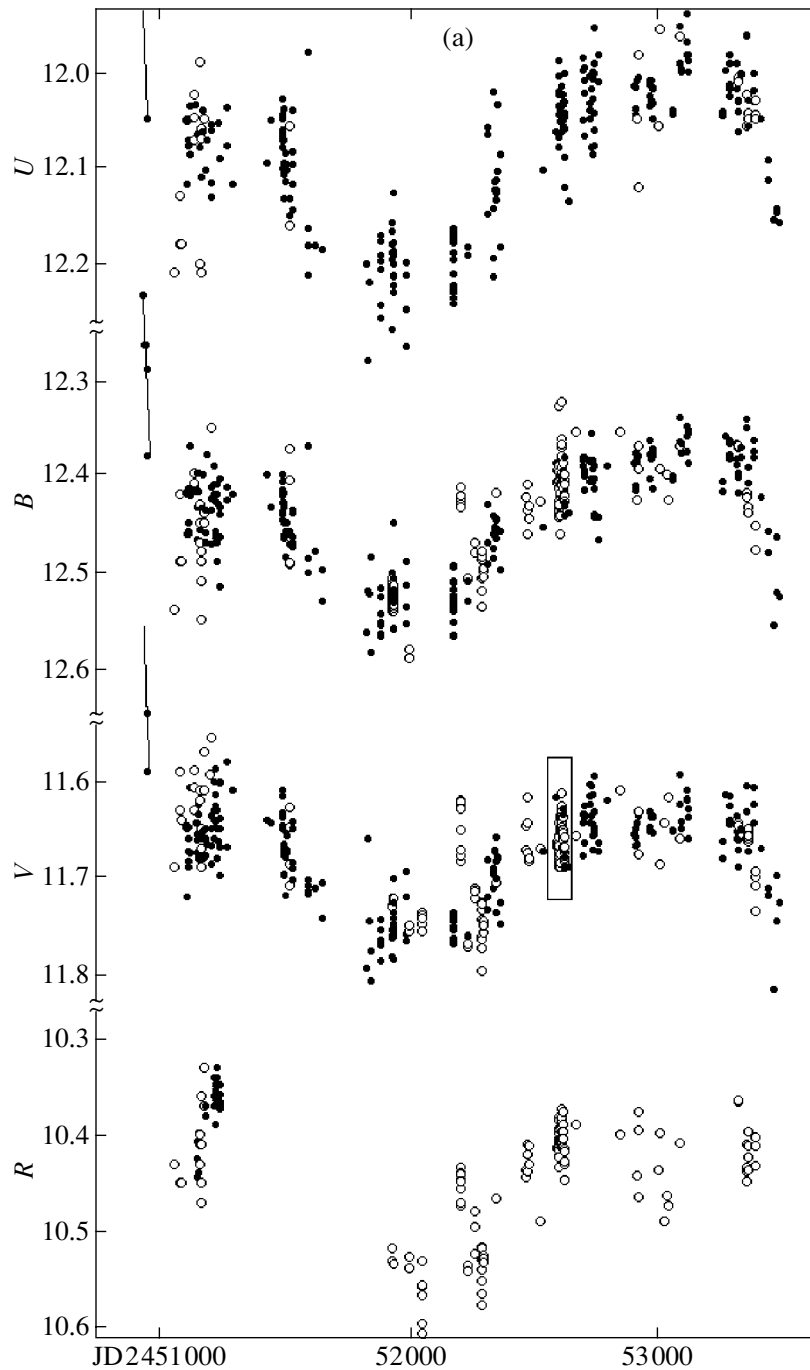


**Fig. 1.** (a) *UBVR* light curves of CI Cam in quiescence after the 1998 outburst. (b) Fragment of the *V* light curve demonstrating periodic low-amplitude variations with  $P \approx 19$  days (enclosed in rectangles in panel (a)).

uniform and had good time coverage, to derive systematic corrections to the non-uniform CCD observations in the *UBV* system. All the other data were reduced to the system for the most uniform Crimean set obtained by Metlova in this way, using observations that were simultaneous or close in time. The  $R_J$  magnitudes for the comparison and control stars,  $9.884^m$  and  $12.034^m$ , respectively, were

determined by us earlier using the SAI 70 cm reflector in Moscow and a single-channel photometer made by I.M. Volkov and S.Yu. Shugarov (an FEU-79 photomultiplier was used to obtain a photometric band close to the Johnson  $R_J$  band). The stars were compared to several stars from the catalog [21]. The characteristic uncertainty of a single photoelectric measurement was  $0.02^m - 0.03^m$ .

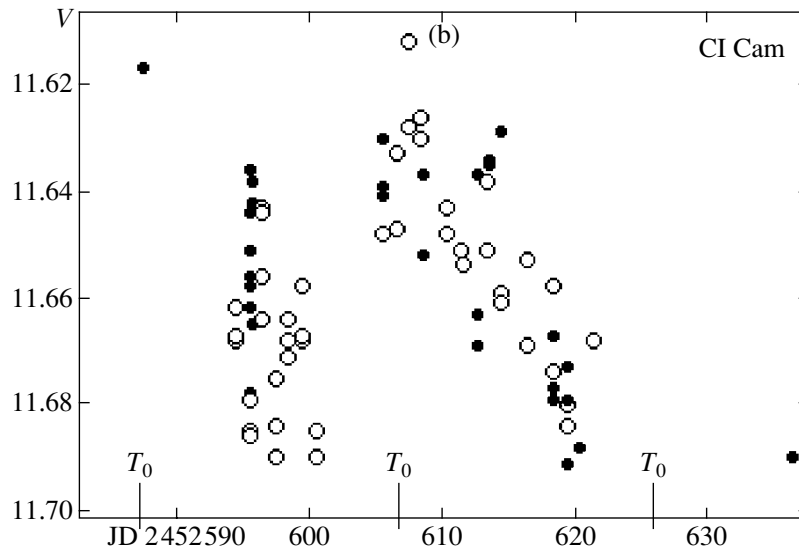


Fig. 1. (Contd.)

CCD observations of CI Cam in the  $UBVR_J$  photometric bands were obtained on the Zeiss-600 telescope of the SAI Crimean Station using SBIG ST-7 and VersArray (Princeton Instruments) chips, as well as on the AZT-5 Maksutov telescope using a Meade Pictor-416 chip at the primary focus. The VersArray photometer was also equipped with a Cousins  $R_C$  filter. The VersArray measurements were obtained using two red filters that approximate the reaction curves of the Johnson and Cousins bands. CCD observations were also acquired in the bands of the  $UBVR_C$  system using the SAO Zeiss-1000 telescope with K585 (“Elektron” Scientific and Industrial Alliance) and EEV 42–40 chips. All the CCD observations were made by E.A. Barsukova and V.P. Goranskii. Certainly, the observations obtained using different chips and filter sets were not uniform, and this situation was made worse by the studied star’s emission spectrum. The reduction of all the data to a single system was comparatively easy for the  $UBV$  bands, thanks to our Crimean data, which made it possible to derive systematic deviations for individual light-curve fragments. Our CCD observations are in a good agreement with photoelectric photometry. It was more difficult to reduce the data acquired in the red filters, including the  $R_C$  filter, to a single  $R_J$  system, and the final light curve may contain some systematic imperfections that could not be removed using simultaneous observations.

The CCD observations were processed using a code written by V.P. Goranskii for the Windows NT environment, which realizes a corrected-aperture measurement method. A table with the original photometric data (before the introduction of the

systematic corrections) can be found at the web address <http://jet.sao.ru/~goray/cicam.all>.

The light curves of the CI Cam in quiescence are shown in Fig. 1a, which plots the photoelectric observations as filled circles and the CCD observations as open circles. The observations joined with solid lines at the beginning of the light curves demonstrate fading at the late stages of the outburst. The brightness variability range after the outburst is  $11.96^m$ – $12.30^m U$ ,  $12.35^m$ – $12.58^m B$ ,  $11.59^m$ – $11.81^m V$ , and  $10.33^m$ – $10.60^m R_J$ . A broad minimum near JD 2451900 was observed in all the filters. In the middle of our last season (February 2005), the star’s brightness began a new steep decline. The scale of the new fading will be revealed in future observations. If the fadings are cyclic, the cycle length should be somewhat longer than the  $1100 \pm 50$  days suggested in [2],  $\approx 1600$  days. Our seven-year observations are not able to confirm the cyclic character of the slow variations, since the cycle did not repeat itself even twice during this interval. In addition to the slow brightness variations, faster changes are observed, resulting in a scatter of  $\approx 0.1^m$  in the light curves in various filters. This scatter could also hide periodic components.

In order to study rapid variations on time scales from several to tens of days and to search for the 11.7-day period found by Miroshnichenko [7], we carried out special frequent observations of the CI Cam at the SAI Crimean Station on 28 nights between November 15 and December 12, 2002 (JD 2452594–2452621). This time interval covers 2.4 of the supposed 11-day periods. Parallel photoelectric and CCD observations were obtained. Our  $V$ -band results are displayed in Fig. 1b. A well-defined wave is apparent

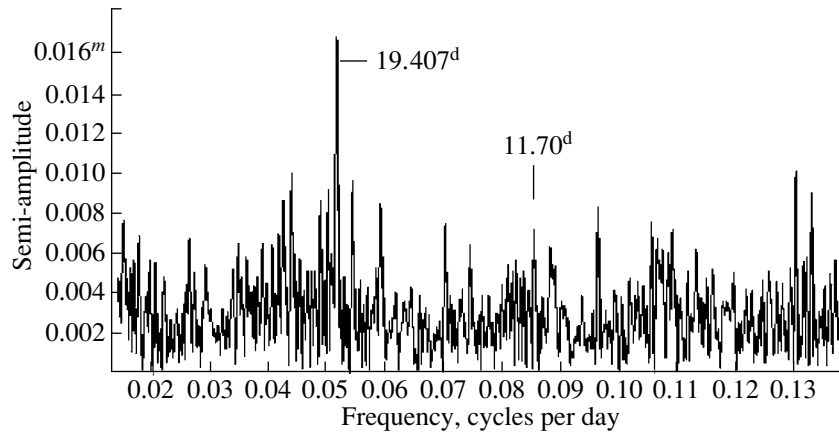


**Fig. 2.** Amplitude–frequency periodogram computed using the Deeming method. The peaks corresponding to the 19.407-day period and the 11.7-day period detected earlier by Miroshnichenko [7] are marked.

in the brightness variations, but with a period that is obviously longer than 11.7 days,  $\approx 19$  days. It turns out that the same period is also present in the other photometric data.

As a preparation for a frequency analysis of the rapid brightness variations, we subtracted a smoothed curve representing the slow trend from the *UBV* light curves. We then applied a frequency analysis using the method of Deeming [22] to the residuals. We carried out calculations both for all-night averages (a total of 172 nights) and for the same data but without the observations from November–December 2002. The amplitude spectrum for all the data is shown in Fig. 2, which is dominated by the peak corresponding to a 19.407-day period (this harmonic’s semiamplitude is  $0.017^m$ ). The uncertainty in

the period estimate is 0.02 days. We have also marked the position corresponding to the 11.7-day period suggested earlier in this figure [2, 7]. It is obvious that the 11-day peak is strongly suppressed by the observations of the last four seasons, but the new 19-day peak is clearly visible. The old observations from the first three seasons do not contradict the 19-day period. The amplitude spectra from the independent series of observations (without November–December 2002) look similar, demonstrating the presence of the 19-day periodicity in all the other observations. Figure 3 shows the light curve folded using the 19.407-day period, where each data point represents an average over a single night. The epoch of maximum indicated by the mean light curve is  $\text{JD}(\text{hel.}) = 2452200.75$ . The solid curve is the mean light curve computed using a moving average.

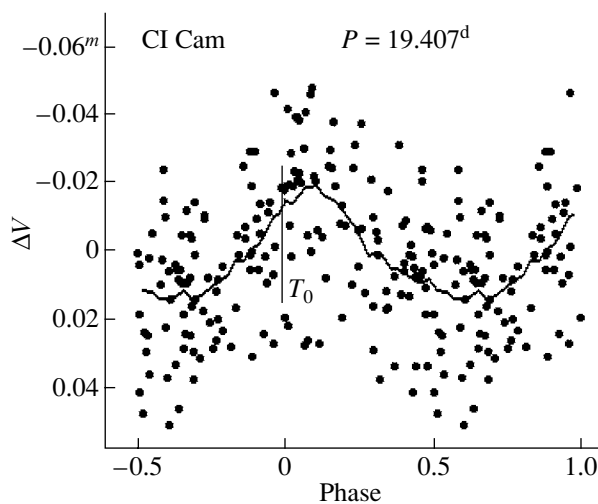


**Fig. 3.** *V*-band residual light curve folded with the 19.41-day period.  $T_0$  is the spectroscopic time of the lower conjunction of the HeII emission source.

### 3. SPECTROSCOPIC OBSERVATIONS

Our spectroscopy of CI Cam began with the SAO 6-m telescope during the outburst, on the night of April 4–5, 1998 using the SP-124 spectrograph, and was continued mainly with the SAO Zeiss-1000 telescope using the UAGS spectrograph and a long slit. The results of the observations made before January 27, 2001 are presented in [2], and a log of the spectra obtained is given in [2, Table 2]. Our spectroscopy of CI Cam during the outburst is described in [2–4, 23, 24].

New medium-resolution ( $4\text{--}10 \text{ \AA}$ ) spectra were obtained in 2001–2005, mainly using the SAO Zeiss-1000 telescope and the UAGS spectrograph. Two spectra with a resolution of  $4\text{--}5 \text{ \AA}$  were taken using the 6-m telescope and the UAGS and SCORPIO spectrographs, especially to achieve a sufficiently high signal-to-noise ratio in the blue.

**Table 1.** Spectroscopic observations of CI Cam

JD(hel.) 24...	Date	Range, Å	Resolution, Å	No. of spectra	Telescope	Observers
52176.467	2001.09.23	4070–5783	8.7	5	1 m	Bu
52176.479	2001.09.23	5626–7330	9.5	7	1 m	Bu
52177.402	2001.09.24	4105–5792	9.5	2	1 m	Bu
52177.500	2001.09.24	5612–7302	6.7	14	1 m	Bu
52189.485	2001.10.06	5610–7317	7.3	8	1 m	Bo
52192.586	2001.10.09	4095–5788	7.0	4	1 m	Bo
52293.428	2002.01.18	4095–5788	7.0	4	1 m	Bo
52299.220	2002.01.24	5655–7359	8.8	17	1 m	Bo
52299.268	2002.01.24	4102–5798	9.5	8	1 m	Bo
52300.409	2002.01.25	3539–4997	0.20	1	6 m	K
52310.470	2002.02.04	4604–6071	0.20	1	6 m	K
52327.251	2002.02.21	4081–5779	8.8	6	1 m	Bo
52327.284	2002.02.21	5626–7332	8.8	10	1 m	Bo
52531.573	2002.09.13	4162–5860	7.0	2	1 m	Bu
52532.520	2002.09.14	4104–5797	9.5	2	1 m	Bu
52532.547	2002.09.14	5622–7328	9.5	6	1 m	Bu
52542.517	2002.09.24	5642–7346	10.1	11	1 m	Bu
52542.554	2002.09.24	4085–5779	10.1	4	1 m	Bu
52598.19	2002.11.19	4558–5996	0.13	1	6 m	K
52683.344	2003.02.12	4090–5784	9.4	6	1 m	Bo
52906.476	2003.09.23	3470–6205	3.7	1	1 m	Bo
52906.492	2003.09.23	3470–6205	3.7	1	1 m	Bo
52906.508	2003.09.23	3470–6205	3.7	1	1 m	Bo
52965.435	2003.11.21	4121–5818	7.5	6	1 m	Bo
53019.304	2004.01.14	3710–7970	7.0	2	1 m	Bu
53023.278	2004.01.18	3710–7997	7.0	3	1 m	Bo
53054.19	2004.02.18	3769–5007	4.3	3	6 m	Ba, Bu, G
53082.346	2004.03.17	3710–8017	7.7		1 m	Bo
53300.435	2004.10.21	3630–7955	7.7	4	1 m	Bu
53301.451	2004.10.22	3850–5922	4.0	2	1 m	Bu
53301.492	2004.10.22	3820–7910	7.7	1	1 m	Bu
53328.330	2004.11.18	3970–5738	5.3	1	6 m	Ba, Bo, G
53357.286	2004.12.17	3800–8090	7.1	7	1 m	Bu
53358.336	2004.12.18	3800–8090	7.1	10	1 m	Bu
53359.354	2004.12.19	3800–8090	7.1	5	1 m	Bu
53360.365	2004.12.20	3800–8090	7.1	2	1 m	Bu
53389.253	2005.01.18	3800–7940	6.2	6	1 m	Bu
53390.279	2005.01.19	3800–7940	6.1	5	1 m	Bu
53417.296	2005.02.15	3800–7910	6.1	2	1 m	Bu
53419.239	2005.02.17	3800–7910	6.2	3	1 m	Bu
53451.245	2005.03.21	3880–6207	6.1	2	1 m	Bu

The observers were E.A. Barsukova (Ba), N.V. Borisov (Bo), A.N. Burenkov (Bu), V.P. Goranskii (G), and V.G. Klochkova (K). The telescopes indicated are the SAO 6 m reflector and the SAO 1 m Zeiss reflector.

The preliminary reduction of all the medium-resolution spectra was carried out in the ESO MIDAS environment using standard techniques. Spectra for individual nights taken for the same positions of the diffraction grating were summed. The wavelength calibration was performed using spectra of a neon–argon lamp. The average sky spectrum was determined from several rows of the CCD chip and subtracted from the star’s spectrum.

Our high-resolution spectra on the SAO 6-m telescope were taken using the NES echelle spectrograph [25] at the Masmith focus, with an EEV 42–40 2048 × 2048 CCD chip. When used with an image slicer [26], the NES spectrograph gives a spectral resolution,  $R \geq 60\,000$ . We obtained three such spectra, two of which were already analyzed in [14].

We reduced our two-dimensional echelle spectra using a modification of the ECHELLE procedure of the MIDAS package [27]. This modification enables the reduction of echelle spectra taken with an image slicer.

The uncertainty in our velocity measurements based on a single line in the spectra taken with the NES spectrograph is 1 km/s.

Finally, all the spectra were continuum-normalized, with the continuum level given a value of unity. Table 1 presents a complete log of the spectra taken from 2001–2005, including the observing dates, spectral regions, and resolutions determined from sky lines. This table is a continuation of Table 2 in [2].

*Fluxes in Emission Lines.* We measured the equivalent widths of the H, HeI, HeII  $\lambda 4686$  Å, FeII, and SiII emission lines and the [NII]  $\lambda 5755$  Å forbidden line, selected for monitoring in [2], and transformed them to fluxes in energy units ( $\text{erg cm}^{-2} \text{s}^{-1}$ ) using the photometric data. To derive the emission-line fluxes in physical units, we determined for each spectrum the contribution of emission lines and the continuum in each filter, converted the photometric magnitudes into flux densities (in  $\text{erg cm}^{-2} \text{s}^{-1} \text{Å}^{-1}$ ) using the data of [28], multiplied these by the contribution from the continuum, and extrapolated the continuum flux densities to the wavelengths of the emission lines. The line fluxes were taken to be the products of their equivalent widths and the continuum flux densities at the wavelength of the line.

The lines selected in [2] are predominantly bright, unblended lines. However, our analysis of the high-resolution spectra sometimes revealed close components that were unresolved in the medium-resolution spectra. If a line was found to be an unresolved blend, the combined equivalent widths of the components were derived.

The brightest line in the optical is H $\alpha$ , whose equivalent width in the star’s quiescent spectrum varies between 350 and 500 Å. This line is usually overexposed in spectra intended for an analysis of weak lines. For this reason, no data on H $\alpha$  were presented in [4]. In some cases, we used short exposures to measure the line’s undistorted intensity. In other instances, when summing the spectrum in rows of the CCD during our reduction, we selected for measurements of EW(H $\alpha$ ) only rows where the line was not overexposed. In this way, we were able to obtain a curve of the intensity variations for the H $\alpha$  emission (Fig. 4a, top). Figure 4a (middle and bottom) shows the analogous relations for the H $\beta$  and H $\gamma$  lines. These relations do not show the cyclic brightenings and fadings characteristic of symbiotic binaries, which are due to reflection from the cool component’s surface. The wave of intensity variations observed in JD 2451090–2451900 can be more adequately interpreted as a rebrightening, followed by a tendency to make a transition to quiescence, with small-amplitude variations. Thus, the wave probably represents a reaction of the gas and dust envelope to the outburst.

The correlation between the hydrogen-line fluxes and the *UBVR* brightness [2] was later disrupted: after the minimum near JD 2451900, there was a brightening and then a broad maximum in the photometric data (Fig. 1a), whereas the line intensities did not show an increase long after the photometric minimum.

Figure 4b displays the intensity variations for the four brightest emission lines of neutral helium. In contrast to the hydrogen lines, these lines’ intensities are well correlated with each other. As for the hydrogen lines, a rebrightening is observed near JD 2451400, but the helium lines demonstrated considerable variations near that time; after the rebrightening, their intensities increased gradually and synchronously. Authors of [4, 23] noted that, after the major outburst of 1998, the HeI emission (in contrast to the HI emission) had faded to a level a factor of 2–10 lower than that observed in the old archive spectra taken before the 1998 outburst. Thus, the gradual brightening of the HeI lines may indicate that the radiation level is approaching the “undisturbed” quiescent state prior to 1998.

The FeII lines, which displayed behavior similar to that of the hydrogen or HeI lines, all behaved similarly after the photometric minimum at JD 2451900: they dropped to an even lower level after which their fluxes stabilized (Fig. 4c).

The [NII]  $\lambda 5755$  Å forbidden line displayed a different behavior than the other lines [2]. During the outburst, the flux in this line remained constant for  $\approx 50^d$ , while the intensities of other emission lines

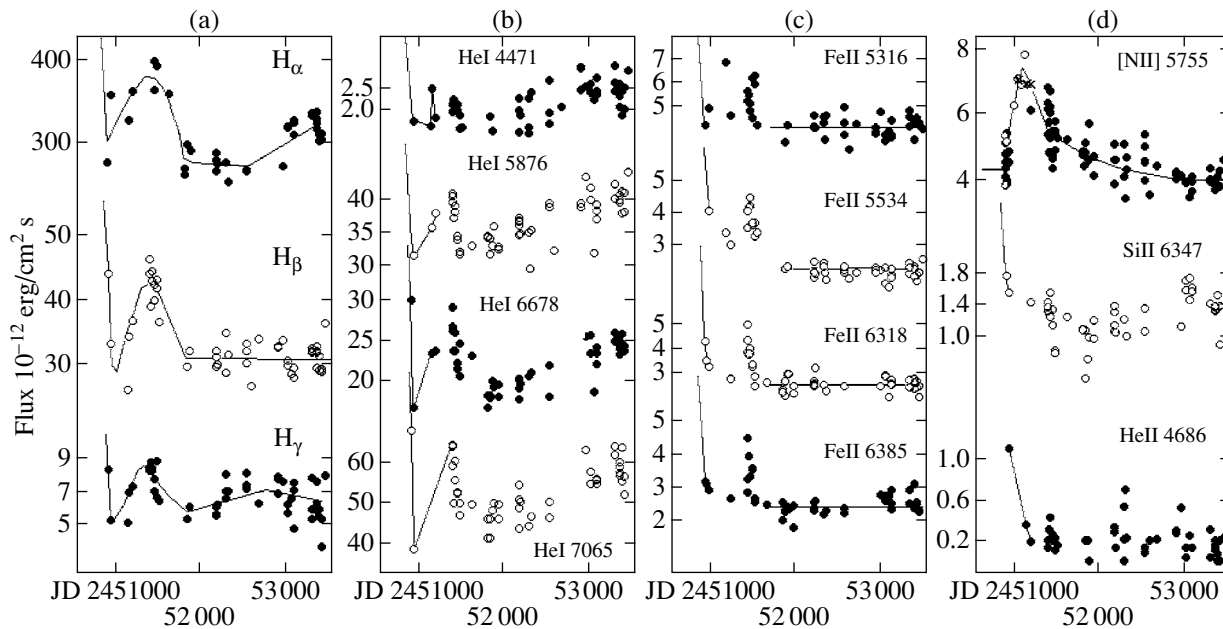


Fig. 4. Flux variations in various emission lines of the CI Cam in quiescence. The solid segments at the beginning of each dependence show the decline of the 1998 outburst.

increased by an order of magnitude or more. 250<sup>d</sup> later, when the fluxes in all the other emission lines had decreased to their normal levels, the [NII] flux increased by a factor of 1.5, and then, by early 2001, decreased to its pre-outburst level. This line is formed in the outmost parts of the gas and dust envelope, where the envelope's density is very low: less than  $10^5$ – $10^6$   $\text{cm}^{-3}$ . Unfortunately, we did not have any observations 50–250 days after the peak of the 1998 outburst. Equivalent widths of the [NII] line for this time range were later published in [4]. We read the equivalent widths from Fig. 5f in [4] and converted them to intensities. Three observations from [11] were also used. The results are shown in Fig. 4d (top). All these data taken together demonstrate that the emission began to brighten 50 days after the outburst peak in the X-ray, with the emission intensity reaching its maximum near JD 2451115 ( $210 \pm 20$  days after the outburst peak). The emission flux was a factor of  $1.8 \pm 0.2$  higher at its maximum than in quiescence. During the following six years, we can trace a gradual fading of this line, whose brightness dropped even somewhat below the level observed during the outburst.

The SiII  $\lambda 6347$  Å line is interesting because, unlike the hydrogen and helium lines, it did not display rebrightening. This is also true of the FeII  $\lambda 6148$  and  $6492$  Å lines. A plot of the SiII intensity variations is shown in Fig. 4d (middle).

The HeII  $\lambda 4686$  Å line has the highest ionization potential among all the lines we measured. At the

outburst peak, the flux in this line increased by a factor of 300 compared to its value in quiescence. It is clear that the HeII line is formed in the immediate vicinity of the compact object in the CI Cam system that was responsible for the outburst. The HeII emission flux quickly reached its quiescent level after the outburst, with its equivalent width fluctuating near  $-0.30$  Å during the last six years. This weak line is not visible in several high-quality spectrograms; one spectrogram, taken on JD 2452310, shows this line's equivalent width to be  $EW = -1.04$  Å corresponding to variability by a factor of three to five.

Thus, our analysis of the intensity variations for emission lines shows a predominant tendency toward stabilization of the structure of the complex, stratified circumstellar envelope after it was distorted by the passage of the outburst shock wave. While the envelope layers emitting in the FeII lines (the slow stellar wind) were already restored three years after the outburst, the HeI emission is still approaching the level that was present prior to the 1998 outburst.

*Balmer-line Diagnostics for the Primary.* Bright absorption wings were found for the H $\delta$  and H $\epsilon$  lines in the spectrum of the CI Cam, which could represent the photospheric absorption of the B star [4]. On February 18, 2004, we obtained a high signal-to-noise ratio spectrum of CI Cam reaching  $\lambda 3679$  Å in the blue with the UAGS spectrograph on the 6-m telescope. High-numbered hydrogen lines, from H $\zeta$  to H $_{10}$ , are visible in this spectrum (Fig. 5a). The spectral resolution is  $4.3$  Å and the full width

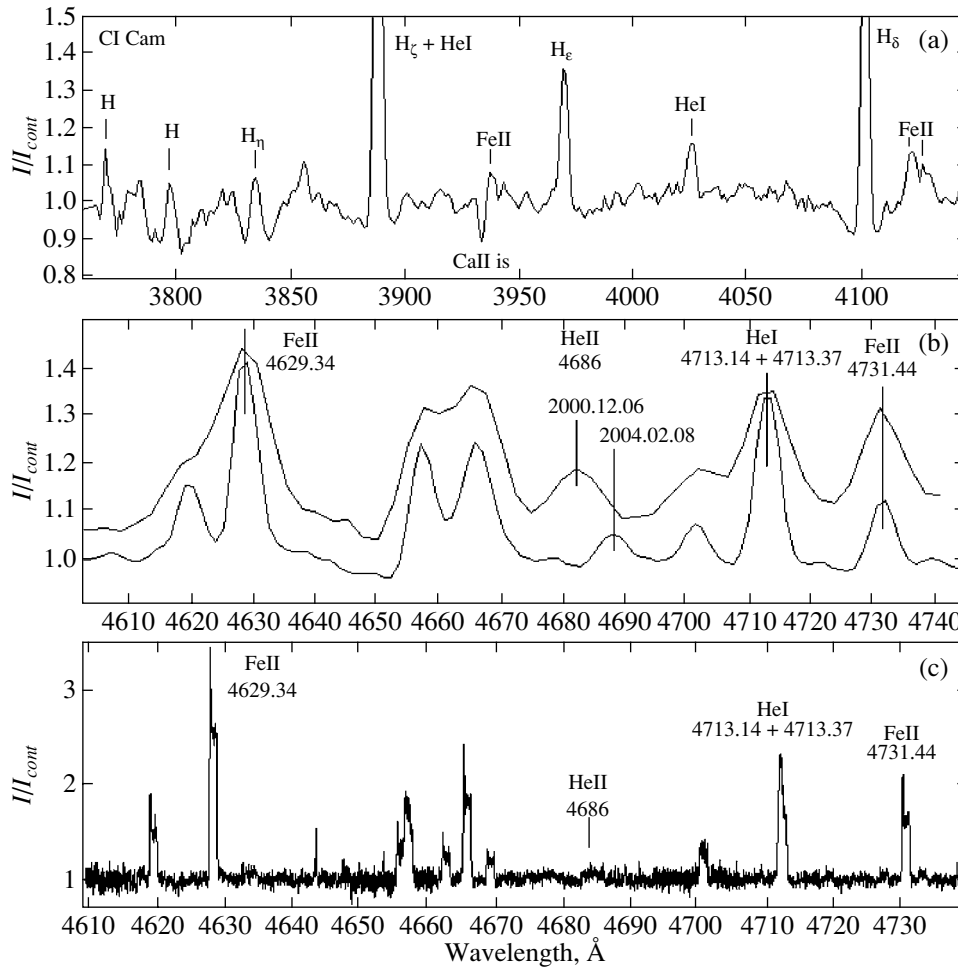


**Fig. 5.** Fragments of the spectra of the CI Cam. (a) A medium-resolution spectrum (6 m/UAGS). Broad absorption wings of the hydrogen lines and the interstellar CaII line are visible. (b) Superposition of two spectra (6 m/UAGS) near the HeII  $\lambda 4686$  Å emission line. A Doppler shift of the HeII line by 400 km/s is evident. (c) A high-resolution spectrum (6 m/NES) near the HeII  $\lambda 4686$  Å emission line.

of the absorption wings at the continuum level is  $FWZI = 25 \pm 2$  Å, whereas the half-width of the emission components is only  $FWHM = 4.8 \pm 0.2$  Å. We can see that the intensities of the hydrogen emission lines decrease steeply with an increasing line number, so that the emission peak is only slightly above the continuum level already in the H $\eta$  profile. The H $\zeta$   $\lambda 3889.051$  Å line is the only one to disagree with this steep relation: it appears brighter and broader, probably due to blending with the strong HeI  $\lambda 3888.646$  Å line. We can determine the spectral type and luminosity class of the CI Cam by comparing the absorption-profile parameters for the CI Cam with profiles for normal B stars of various luminosity classes. It is obvious that we cannot use the full-width at half-maximum, FWHM, of the absorption component for this purpose, because the central parts of the profiles are distorted by emission. However,

full-width parameter FWZI can be used, since it can be determined without knowing the line depth, and the narrow emission component does not distort the outer parts of the line's broad wings. However, the resulting uncertainties in FWZI are an order of magnitude higher than uncertainties in FWHM.

We selected the H $\delta$   $\lambda 4101.74$  Å and H $\eta$   $\lambda 3835.39$  Å lines, whose absorption wings are least distorted by emission lines of the circumstellar envelope. Figure 5a shows that only one weak, narrow line, possibly CrII  $\lambda 4112.59$  Å, overlaps the red H $\delta$  wing, and this feature presents no obstacle for estimating the full width of the H $\delta$  line.

We derived relations for the hydrogen-line widths and half-widths in the B-star spectra using the stellar spectra from the databases [29, 30]. Our control star was HD 52918 (Sp = B1V), for which a spectrogram

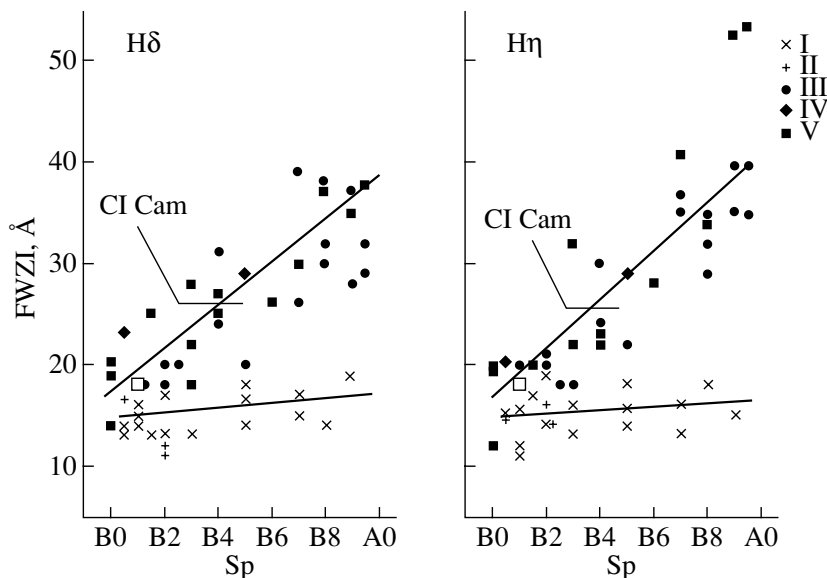


Fig. 6. Full widths of the  $H\delta$  and  $H\eta$  lines in the spectra of B stars as functions of their spectral type and luminosity class.

was taken on the same night and with the same instrument. On average, the spectral resolution in [29] is  $4.5 \text{ \AA}$ , close to our value ( $4.3 \text{ \AA}$ ). The spectra in [30] have a better spectral resolution ( $2.9 \text{ \AA}$ ). We reduced the values of FWZI and FWHM for these data to the poorer spectral resolution,  $4.3 \text{ \AA}$ , assuming that both the lines themselves and the instrumental profiles were Gaussian. We determined the line FWHM values using the CENTER/GAUSS option of the MIDAS package. There are some arbitrary aspects to determining the line widths: the full width depends on the adopted continuum level, and has uncertainties of  $2\text{--}3 \text{ \AA}$ . However, the existence of a clear correlation between FWZI and FWHM confirms the reliability of our estimates.

The result of our database analysis — the dependence of the  $H\delta$  and  $H\eta$  line widths on the spectral type and luminosity class — is shown in Fig. 6, where class I and II supergiants are shown by crosses and plus signs, and class III, IV, and V stars are shown by circles, diamonds, and squares. The open square marks the position of our control star, HD 52918. The figure shows that the minimum difference in the line widths for different luminosity classes is observed only for the hottest B stars (B0–B2). The line-width differences between luminosity classes I–II and III–V increase for later spectral types, although we see no significant differences between classes I and II or among classes III–V. With its absorption-wing width of  $25 \text{ \AA}$ , the CI Cam has a position far outside the region occupied by supergiants, and its spectral type can be unambiguously determined as B4III–V. The absolute magnitudes for such stars,  $M_V$ , can be between  $-1.2^m$  and  $-2.3^m$  [31], and the implied

distance calculated with the adopted interstellar reddening,  $E(B-V) = 0.85^m$ , is  $1.1\text{--}1.9 \text{ kpc}$ .

According to [5], the ultraviolet spectrum of CI Cam at  $\lambda 1250\text{--}2650 \text{ \AA}$  agrees well with the spectrum of BD+33°2642 (B3IV) [5, Fig. 5]. The spectral type B3IV agrees with our own estimate, B4III–V, within errors. Nevertheless, the CI Cam was classified as a supergiant in [5] based on other criteria, implying a distance in excess of  $5 \text{ kpc}$ .

*The Orbital Period of the CI Cam.* Most spectral lines of the CI Cam in quiescence show no considerable radial-velocity variations. The FeII emission lines formed in the stellar wind have rectangular profiles with widths of  $1.2 \text{ \AA}$ . The radial velocities for these lines' centers based on our echelle spectra and published data range between  $-46$  and  $-51 \text{ km/s}$ , consistent with the observational uncertainties. However, we noticed that the HeII  $\lambda 4686 \text{ \AA}$  line showed Doppler shifts of more than  $400 \text{ km/s}$  relative to adjacent lines (Fig. 5b).

To improve the accuracy of the radial velocities based on the HeII  $\lambda 4686 \text{ \AA}$  line, we derived differential radial-velocity measurements for this line relative to the relatively stationary nearby FeII lines. A fragment of a high-resolution spectrum (Fig. 5c) shows suitable isolated lines, FeII  $\lambda 4629.34$  and  $4731.44 \text{ \AA}$ , in the vicinity of the HeII line. We used the close blend, HeI  $\lambda 4713.14+4713.37 \text{ \AA}$ , as a control line to estimate the uncertainties in our radial-velocity measurements and to monitor the velocity stability of the FeII lines.

We found that the shifts of the HeII line depend on the phase of the  $19.41\text{-day}$  photometric period

**Table 2.** Radial velocities and equivalent widths of the HeII  $\lambda 4686 \text{ \AA}$  and HeI  $\lambda 4713 \text{ \AA}$  lines

JD(hel.) 24...	Phase	$V_r$ , km/s		$Q$	EW, $\text{\AA}$	
		HeII	HeI		HeII	HeI
50908.260	0.490	-93	-85	10	-33.27	-17.11
50909.190	0.538	-116	-81	10	-38.82	-20.15
50910.200	0.590	-106	-106	10	-47.24	-22.42
50923.250	0.262	-59	-74	10	-4.74	-1.27
50950.307	0.656	-86	-79	10	-1.59	-1.35
51150.338	0.964	-104	-59	3	-0.53	-1.80
51204.333	0.746	-96	-66	7	-0.28	-1.94
51399.525	0.804	-106	-81	3	-0.19	-1.56
51400.510	0.855	-143	-21	6	-0.28	-2.05
51423.566	0.043	187	-36	5	-0.43	-1.03
51424.551	0.094	-16	-33	2	-0.31	-2.40
51426.582	0.198	128	-59	5	-0.60	-2.27
51464.542	0.154	247	-41	1	-0.37	-2.16
51465.434	0.200	-34	-51	2	-0.28	-1.10
51485.653	0.242	169	-21	3	-0.16	-1.68
51488.447	0.386	61	-50	6	-0.33	-1.50
51514.288	0.718	-151	-66	4	-0.23	-1.35
51844.500	0.733	-124	-40	8	-0.32	-1.18
51864.448	0.761	-76	-98	3	-0.31	-1.35
51885.319	0.836	-244	-74	9	-	-
52176.467	0.839	-244	-97	3	-0.52	-1.40
52177.402	0.887	-344	-116	3	-0.45	-1.11
52192.586	0.669	-51	-29	2	-0.20	-1.40
52293.428	0.866	-188	-106	3	-0.80	-1.64
52299.268	0.167	-4	-149	1	-0.33	-1.23
52300.409	0.225	-	-51	0	0.00	-2.12
52310.470	0.744	-146	-62	10	-1.04	-1.35
52327.251	0.609	-196	-16	1	-0.35	-1.55
52531.573	0.137	129	-51	1	-0.20	-1.5
52542.554	0.703	-184	-132	2	-0.13	-1.68
52598.190	0.570	-70	-63	10	-0.28	-1.41
52683.344	0.958	-190	-52	4	-0.30	-2.28
52906.476	0.455	-81	-65	9	-0.37	-2.14
52906.492	0.456	-66	-68	9	-0.38	-2.12
52906.508	0.457	-51	-60	9	-0.40	-2.22

**Table 2.** (Contd.)

JD(hel.) 24...	Phase	$V_r$ , km/s		$Q$	EW, Å	
		HeII	HeI		HeII	HeI
52965.435	0.494	4	-166	4	-0.70	-2.80
53019.304	0.269	-19	-39	1	-0.05	-1.52
53023.278	0.474	4	-46	3	-0.18	-1.37
53054.190	0.067	113	-60	10	-0.33	-1.60
53082.346	0.518	-121	-43	4	-0.18	-1.83
53300.435	0.756	-	-66	0	0.00	-1.48
53301.449	0.808	-243	-11	4	-0.41	-1.90
53357.286	0.685	-332	-49	2	-0.28	-1.82
53358.336	0.739	-336	-66	3	-0.15	-2.05
53359.354	0.792	-86	-74	2	-0.21	-2.00
53360.365	0.844	-251	-61	1	-0.20	-2.22
53389.253	0.332	24	-71	1	-0.11	-2.10
53390.279	0.385	-	-51	0	0.00	-1.92
53417.296	0.777	-	-51	0	0.00	-2.41
53419.239	0.878	-114	-14	1	-0.27	-2.92
53451.245	0.527	-29	-77	3	-0.33	-2.73

(Fig. 7a). The radial-velocity curve for the CI Cam based on the HeII 4686 Å line is saw-tooth shaped, testifying that the orbit is elliptical and that the passage of the orbit periastron occurs near the lower conjunction of the HeII emission source (the longitude of the ascending node of the orbit is  $\omega \approx 270^\circ$ ). The HeI line exhibits no Doppler shifts and no dependence on the phase of the 19-day period, with its radial-velocity dispersion being 23 km/s (Fig. 7b). Some spectra show deviations of the HeI radial velocity exceeding 100 km/s, possibly due to observational errors.

The HeII  $\lambda 4686$  Å line is very weak in quiescence, sometimes at the noise level. It was not detected in four of our spectra. Radial-velocity measurements for such a weak line can have a low accuracy. To test this, we estimated the quality of the line profile in each spectrum using parameter  $Q$  ranging from 1 to 10. If a profile was symmetric, bell-shaped, and had a high intensity, it received a  $Q$  value of 10; if the line was detectable only as a weak fluctuation against noise, it received a  $Q$  value of 1; asymmetric profiles or profiles with intermediate levels of noise distortion received intermediate values. These estimates are reflected using circles with different radii in the radial-velocity curve (Fig. 7), so the size of a circle is proportional to the profile quality  $Q$ , and

thereby the accuracy in the radial velocity. Only observations obtained during quiescence are shown in Fig. 7. The observations obtained during the outburst display no phase dependence, and the corresponding radial velocities are close to  $-100$  km/s. Note that the X-ray peak occurred at orbital phase 0.30, and that the intensity of the HeII 4686 Å emission increased by the factor of 300 at the peak of the 1998 outburst.

The numerical results are presented in Table 2, whose columns contain the (1) Julian (heliocentric) dates, (2) phases of the 19.4-day period, (3) radial velocities of the HeII line emission, (4) radial velocities based on the HeI line emission, (5) estimates of the HeII profile quality ( $Q$ ), and (6), (7) the equivalent widths of the HeII and HeI emission lines.

We used the technique described in [32] to estimate spectroscopic orbital elements (Table 3). The semiamplitude of the radial-velocity curve is  $K_x = 230 \pm 50$  km/s. The model radial-velocity curve that best agrees with the observations (solid curve in Fig. 7a) implies an orbital eccentricity of 0.62. The orbit's semimajor axis is  $a \sin i \approx 48 \times 10^6$  km. In this case, the height of periastron above the center of the primary (B[e] star) is  $h \sin i \approx 15 \times 10^6$  km. The parameter  $h$  constrains radius estimates for the B[e] star. Since the radii of supergiants are  $(24-32) \times$

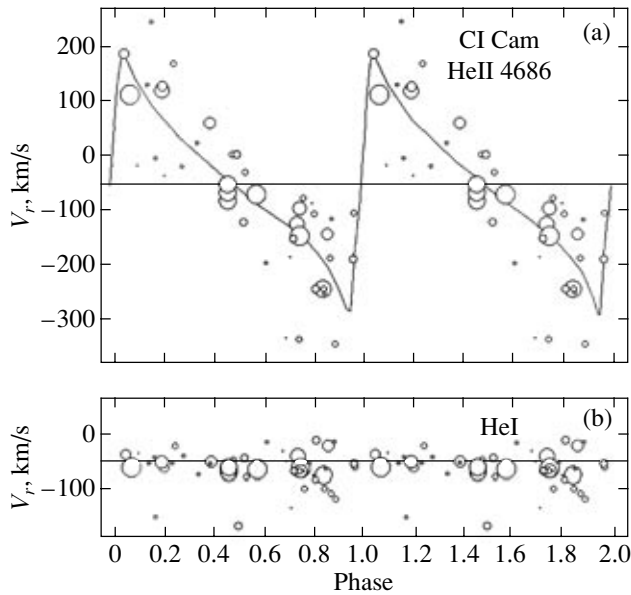


**Fig. 7.** Radial-velocity curves for the (a) HeII line and (b) HeI blend as functions of the phase of the 19.407-day orbital period. The sizes of the circles reflect the quality of the measured HeII line profile and the accuracy of the radial-velocity measurements (see text). The solid curve is the theoretical radial-velocity curve for the adopted spectroscopic elements.

$10^6$  km [31], the CI Cam primary can be a supergiant only if the orbital inclination is small ( $i < 35^\circ$ ), based solely on the condition that the orbit be above the stellar surface. The radius of a B4III–V star can be  $(2.5\text{--}4.1) \times 10^6$  km. Thus, the spectral type we have derived does not contradict the orbital elements for any orbital inclination.

Although we have no observations near the compact component’s lower conjunction, the epoch of the lower conjunction can be refined using observations at nearby phases. The refined epoch of the

**Table 3.** Spectroscopic elements of CI Cam

Sp	B4III–V[e] + WD
$P_{orb}$	$19.407 \pm 0.020$ days
$K_x$	$230 \pm 50$ km/s
$K_{B[e]}$	$< 5$ km/s
$e$	0.62
$\omega$	$\approx 270^\circ$
$T_0$	JD 2452199.0
$a \sin i$	$48 \times 10^6$ km
$f_x(M)$	$12 M_\odot$

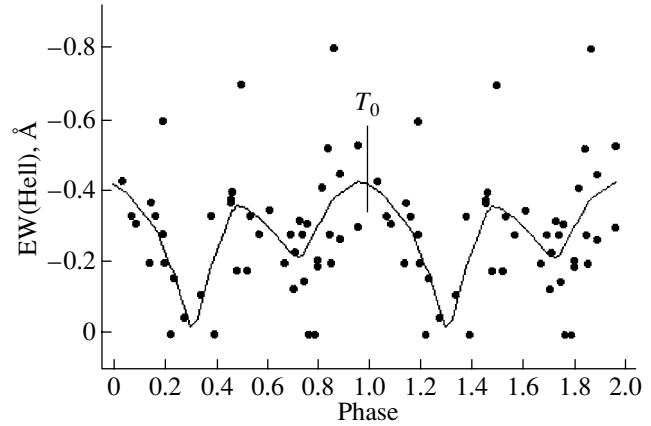


**Fig. 8.** Phase dependence of the equivalent width of the HeII  $\lambda 4686$  Å line. The solid curve is the mean relation smoothed using moving averages.  $T_0$  is the spectroscopic epoch of the lower conjunction for the source of the HeII emission.

lower conjunction for the HeII emission source is  $\text{JD } 2452199.0 \pm 0.2$ . The light-curve phases in Fig. 3 were calculated relative to this epoch, and the phase of the lower conjunction is labeled  $T_0$  in this figure. It appears that the phase of the maximum occurs  $0.09 P$  (1.75 days) later than the lower conjunction, virtually at the epoch of the highest recessional velocity of the orbiting object.

The origin of the low-amplitude orbital variability is not yet clear, but it is evident that the increase in the system’s brightness is observed some time after the closest approach of the compact object to the B star, rather than exactly at periastron. During the approach to periastron, the stellar-wind density and the velocity of the compact component increase. If the compact component is surrounded by an accretion disk, the surface of this disk may become brighter due to interaction with the stellar wind. At the same time, the stellar wind in the CI Cam system is not radially symmetrical, and its slow component is concentrated toward the equatorial plane. The model profiles for optically thin lines formed in a “disklike wind” for inclinations of the stellar rotational axis of  $45^\circ\text{--}60^\circ$  calculated in [33] resemble the three-peaked profiles of the disk lines of the CI Cam [14]. One appreciable difference between the real and model profiles is that the observed red peak is considerably weaker than the blue peak, but this could be explained by internal absorption in the circumstellar matter, or by screening of part of the disklike wind by the B star itself. Thus, the phase shift between the photometric curve and the radial-velocity curve may indicate that the system is brightest during the passage of the compact component through the equatorial plane of the B star, soon after it has made its closest approach to this star.

It follows from the phase dependence of the HeII emission-line equivalent widths that one of the local maxima in this quantity is observed near  $T_0$ . The dependence displays a double wave, with two local minima near  $\phi = \pm 0.25 P$  (Fig. 8). The spectra with undetectable HeII emission were also taken at phases near these minima. The dependence displays considerable scatter, and it is not clear how significant the discussed features are. For this reason, it is important to refine this relation before trying to interpret it. However, one conclusion based on the phase dependence of the HeII line equivalent widths is obvious: the disappearance of the lines is not due to an eclipse of the compact component by the B star, and no such eclipse is observed at the expected phase.

The absence of Doppler shifts of the bright lines (H, HeI, and FeII) in excess of several km/s is a well-established observing fact, although the wind lines of the B star should reflect its orbital motion. This obviously means that the mass of the compact component in the CI Cam system is significantly—by more than a factor of 46—lower than the mass of the B-star primary. The equatorial-wind velocity measured for the CI Cam based on the profiles of iron lines is only 32 km/s [5]. At the same time, high-velocity spectra demonstrate that the structure of these profiles is very stable in quiescence. The fact that the compact component's motion does not disturb the structure of such a slow stellar wind also testifies to a low mass for this component. The mass function of the compact component is  $f_x(M) = 12 M_\odot$ ; this is a *lower limit* for the mass of the primary. In this study, we established based on the Balmer absorption widths that the CI Cam primary has spectral type B4III–V. The expected masses for such stars do not exceed  $7 M_\odot$ , while their radii should be no larger than  $6 R_\odot$  ( $4.5 \times 10^6$  km). Thus, the star's photospheric spectrum contradicts the dynamical estimate of its mass. We believe this contradiction comes about because the B star in the CI Cam system is not a normal main-sequence star, but instead an evolved, hydrogen-poor, underluminous star that has already spent its hydrogen fuel. Apparently, at the start of its evolution, the low-mass compact component had a higher mass than the present primary. It completed its evolution to the compact state, losing nearly all of its mass, which was partially transferred to the B star observed now.

Our observations also provide information about the nature of the compact component. The Doppler shifts displayed by the wind lines of the system's primary in high-dispersion spectra obviously do not exceed 10 km/s; thus, we can conclude from the ratio of the radial-velocity semi-amplitudes that the mass of the compact component is at least a factor of 46

lower than the mass of the primary, and  $M_x \sin^3 i < 0.26 M_\odot$ . Hence, if the orbital inclination is  $i > 38^\circ$ , the mass of the compact object is below the Chandrasekhar limit, and the compact component is a white dwarf. If the (unknown) orbital inclination is lower, there is a low probability that the compact object is a neutron star. The presence of a black hole in the CI Cam system is the least probable. The source of the weak HeII emission is probably an accretion disk around the white dwarf.

X-ray observations during the outburst and in quiescence [11, 12] also testify to the CI Cam secondary as a white dwarf, with the 1998 outburst being due to a thermonuclear explosion of fuel accumulated on its surface. In the case of classic novae, the gas shell consisting of the explosion products expands into empty space, undergoing in succession the optically-thick, recombination, optically-thin, and nebular stages. In the CI Cam, we observed a thermonuclear explosion in a dense circumstellar medium; the difference from classic novae is the interaction with the medium and deceleration of the explosion products [13], as well as the absence of a nebular stage. The radio observations of [13] demonstrate a bipolar structure of the ejecta and the shock propagation. We believe this structure of the ejecta could be due to the existence of an accretion disk around the white dwarf, which stopped the propagation of the explosion products near the plane of the disk, and the disk was not destroyed in the outburst.

#### 4. CONCLUSIONS

The main conclusions of our study are the following.

- (1) Intensity variations of emission lines over the last seven years demonstrate a predominant tendency toward stabilization of the complex, stratified circumstellar envelope of CI Cam after this structure was disturbed by the passage of the outburst shock wave.
- (2) We have classified the CI Cam primary as a B4III–V star, based on an analysis of the hydrogen absorption lines. The spectroscopic distance to such a star is 1.1–1.9 kpc.
- (3) We have determined the orbit of the compact component in the CI Cam system, which has a period of  $19.41 \pm 0.02$  days and an eccentricity of 0.62. The light curve exhibits a low-amplitude wave with this orbital period.
- (4) The photospheric spectrum of the primary, B4III–V, is in contradiction with its estimated dynamical mass,  $M(B[e]) > 12 M_\odot$ . This contradiction can be removed if the star has undergone prolonged evolution in a binary system with mass exchange.

## ACKNOWLEDGMENTS

This project (E.A.B. and V.P.G.) was supported by the Russian Foundation for Basic Research (project codes 03-02-16133, 03-02-16580, and 05-02-26843-z). V.G.K. thanks the CRDF foundation (project 14651).

## REFERENCES

1. H. J. G. L. M. Lamers, F.-J. Zickgraf, D. de Winter, et al., *Astron. Astrophys.* **340**, 117 (1998).
2. E. A. Barsukova, N. V. Borisov, V. P. Goranskii, et al., *Astron. Zh.* **79**, 309 (2002) [*Astron. Rep.* **46**, 275 (2002)].
3. J. S. Clark, A. S. Miroshnichenko, V. M. Larionov, et al., *Astron. Astrophys.* **356**, 50 (2000).
4. R. I. Hynes, J. S. Clark, E. A. Barsukova, et al., *Astron. Astrophys.* **392**, 991 (2002).
5. E. L. Robinson, I. I. Ivans, and W. F. Welsh, *Astrophys. J.* **565**, 1169 (2002).
6. A. S. Miroshnichenko, *Odessa Astron. Publ.* **7**, 76 (1994).
7. A. S. Miroshnichenko, *Astron. Astrophys. Trans.* **6**, 251 (1995).
8. J. Zorec, *B[e] Stars*, Ed. by A. M. Hubert and C. Jaschek (Kluwer, Dordrecht, 1998), p. 27.
9. Ya. N. Chkhivadze, *Astrofizika* **6**, 65 (1970).
10. T. Belloni, S. Dieters, M. E. van den Ancker, et al., *Astrophys. J.* **527**, 345 (1999).
11. M. Orlandini, A. N. Parmar, F. Frontera, et al., *Astron. Astrophys.* **356**, 163 (2000).
12. M. Ishida, K. Morio, and Y. Ueda, *Astrophys. J.* **601**, 1088 (2004).
13. A. J. Mioduszewski and M. P. Rupen, *Astrophys. J.* **615**, 432 (2004).
14. A. S. Miroshnichenko, V. G. Klochkova, K. S. Bjorkman, and V. E. Panchuk, *Astron. Astrophys.* **390**, 627 (2002).
15. R. M. Hjellming, A. J. Mioduszewski, Y. Ueda, et al., *IAU Circ.* **6872** (1998).
16. R. M. Hjellming and A. J. Mioduszewski, *Sky Telescope* **96** (2), 22 (1998).
17. M. P. Rupen, A. J. Mioduszewski, and R. M. Hjellming, *New Views of Microquasars*, Ed. by Ph. Dourouchoux et al. (Center for Space Physics, Kolkata, 2002), p. 221.
18. Yu. K. Bergner, A. S. Miroshnichenko, R. V. Yudin, et al., *Astron. Astrophys., Suppl. Ser.* **112**, 221 (1995).
19. T. Kato and M. Uemura, *Inform. Bull. Var. Stars* **5081** (2001).
20. E. A. Barsukova, N. V. Borisov, A. N. Burenkov, et al., *Astron. Telegram* **416** (2005).
21. V. G. Kornilov, I. M. Volkov, A. I. Zakharov, et al., *Tr. Gos. Astron. Inst. im. P.K. Shternberga* **63** (1991).
22. T. J. Deeming, *Astrophys. and Space Sci.* **36**, 173 (1975).
23. E. A. Barsukova, S. N. Fabrika, S. A. Pustilnik, and A. V. Ugryumov, *Bull. Spec. Astrophys. Obs.* **45**, 147 (1998).
24. E. A. Barsukova and S. N. Fabrika, *Variable Stars: Key to Understanding the Structure and Evolution of the Galaxy*, Ed. by N. N. Samus' and A. V. Mironov (Cygnus, Nizhnii Arkhyz, 2000), p. 154 [in Russian].
25. V. E. Panchuk, N. E. Piskunov, V. G. Klochkova, et al., Preprint № 169, SAO (Special Astrophysical Observatory, Nizhnii Arkhys, 2002).
26. V. E. Panchuk, M. V. Yushkin, and I. D. Naidenov, Preprint № 179, SAO (Special Astrophysical Observatory, Nizhnii Arkhys, 2003).
27. M. V. Yushkin and V. G. Klochkova, Preprint № 206, SAO (Special Astrophysical Observatory, Nizhnii Arkhys, 2004).
28. V. Straizys, *Multicolor Stellar Photometry* (Mokslas, Vilnyus, 1977; Pachart Publ. House, Tucson, 1992), p. 139.
29. G. H. Jacoby, D. A. Hanter, and C. A. Christian, *Astrophys. J., Suppl. Ser.* **56**, 257 (1984).
30. J.-F. Le Borgne, G. Bruzual, R. Pello, et al., *Astron. Astrophys.* **402**, 433 (2003).
31. V. Straizhis, *Metal-Deficient Stars* (Mokslas, Vilnyus, 1982) [in Russian].
32. M. G. J. Minnaert, *Practical Astronomy* (Mir, Moscow, 1971; D. Reidel Publishing Co., Dordrecht-Holland, 1969).
33. F.-J. Zickgraf, *Astron. Astrophys.* **408**, 257 (2003).

*Translated by N. Samus'*